Younger, but not older, brains are poised at a critical point of functional activity

Corey Weistuch,[1,2] Lilianne R Mujica-Parodi,[1,3,4,5,6] Anar Amgalan,[1,3,5] and Ken A Dill[1,5,7,*]

[1] *Laufer Center for Physical and Quantitative Biology, Stony Brook University*
[2] *Department of Applied Mathematics and Statistics, Stony Brook University*
[3] *Department of Biomedical Engineering, Stony Brook University*
[4] *Program in Neuroscience, Stony Brook University*
[5] *Department of Physics and Astronomy, Stony Brook University*
[6] *Athinoula A. Martinos Center for Biomedical Imaging, Massachusetts General Hospital and Harvard Medical School*
[7] *Department of Chemistry, Stony Brook University*[*]

(Dated: April 23, 2020)

Aging is associated with significant changes in communication between brain regions, yet the principles governing these changes are poorly understood. Here, we examined the role of age-related glucose hypometabolism by adapting functional MRI data to the Ising model. We found that younger, but not older, brains are poised at a critical point, facilitating switching between specific patterns of integrated and segregated activity, and consistent with decreased energy availability.

Aging is associated with weakened communication between brain regions, or *functional connectivity* (FC) [1, 2]. Recent experiments utilizing positron emission tomography (PET) have shown that the regions most affected by aging, such as the hippocampus, not only have disproportionately large energy requirements but also are most susceptible to decreased glucose utilization ("hypometabolism") [3]. Thus, it has been proposed that weakened FC, specifically regional signal correlations from functional magnetic resonance imaging (fMRI), may reflect the brain's adaptation to reduced energy availability [3, 4]. However, the strategy the brain takes to toggle these connections is currently unknown.

At rest (i.e., when no explicit task is being done), brain activity alternates between *segregating* computations to distinct, functional domains and *integrating* this information across these domains [4–7]. Metabolic demand increases in proportion to the number and length of functional connections [8]. Therefore, integrated activities, which correspond to highly-connected functional networks, should be exceptionally costly [5]. In fact, these connections have been shown to be the first to weaken with age [4, 9]. Thus, declining glucose metabolism in older brains would bias brain activity to selectively utilize lower-cost, segregated networks.

To test this hypothesis and more fully characterize its emergent, whole-brain consequences, we analyzed two fMRI datasets. The first is the *lifespan* Cam-CAN open-source 3T fMRI resting-state dataset of 636 individuals, ranging over ages 18-88 [10]. The second, which holds age constant in order to isolate the effects of energy alone, is our own *metabolic* 7T fMRI within-subject experiment, of 12 healthy young adults on glycolytic and ketogenic diets. Ketone bodies increase the Gibbs free energy change of ATP production by 27% as compared to glucose [11], with associated increases in cardiac efficiency [11] and brain activity [12]. Thus, if the network changes with age (young to old) indeed result from a metabolic deficit, we should see the opposite effect when switching from lower-energy glucose to higher-energy ketone metabolism.

To predict how different metabolic conditions modulate whole-brain emergent activity, we exploit the advantages of a generative biophysical model by directly mapping our fMRI data onto the *Ising model* [13, 14]. The Ising model provides emergent effects in the form of occupation probabilities of different functional patterns. Widely used in physics, the Ising model is the simplest model describing how pairwise interactions (or couplings) among microscopic, binary (± 1) elements give rise to macroscopic behaviors, including correlations ([13], **Supplementary Fig. 1**). Here our "microscopic" elements are the 498 Willard Atlas brain regions measured in fMRI experiments, each of which is initially assumed to be connected to every other with the same coupling strength (**Extended Data Fig. 1**). The "macroscopic" behavior of interest is the observed network *synchrony*, s, or the average activity across all regions [15, 16]. To explore this model, we find the value of the relative coupling, Λ, that best fits the experimentally observed synchrony values for each subject. In this way we learn how Λ depends on both age and available energy (for detailed methods, see **Supplementary Fig. 2**). Here, each value of s corresponds to the degree of order of a particular network produced by the best-fitting Ising model [16]. As a model-validation step, we find that the Ising model correctly captures higher-order features of $P(s)$, across age and metabolic conditions, that could not be predicted from correlations alone (**Extended Data Fig. 2**).

The Ising model is particularly useful in understanding how small changes in microscopic properties (such as a coupling) can give rise to abrupt and qualitatively distinct macroscopic changes (i.e., emergent effects). In the Ising model, couplings (assumed positive) control the occupation probabilities of different networks. When couplings are large, ordered networks ($s = \pm 1$) are most likely, and when they are small, random disordered net-

[*] dill@laufercenter.org

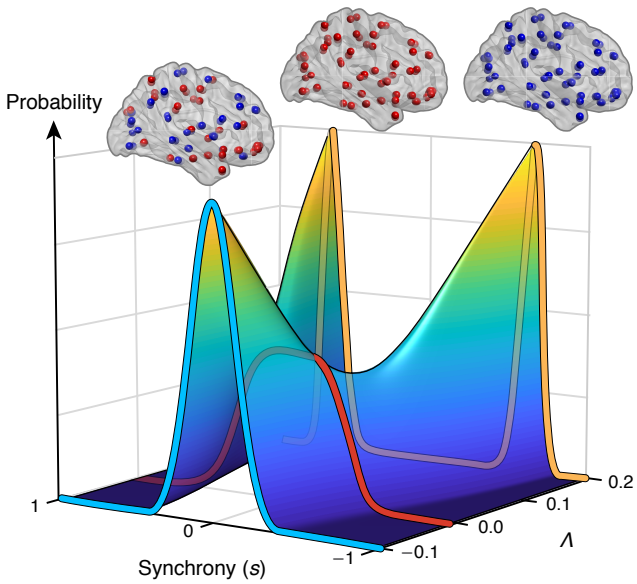

Figure 1 The Ising model applied to brain synchrony. Shown is the probability distribution of different values of synchrony (s) for different values of the dimensionless quantity Λ, reflecting the distance of the actual coupling, λ from the critical point λ_c: $\Lambda = (\lambda - \lambda_c)/\lambda_c$. For $\Lambda < 0$ (weak coupling), there is a single unimodal population having a peak at $s = 0$ (blue line). For $\Lambda > 0$ (strong coupling), the population is bimodal, with a peaks at $s \gg 0$ and $s \ll 0$ (orange line). Above each peak is a typical network; nodes are brain regions and colors are states (red +1, blue −1). $\Lambda = 0$ defines the critical point, where $s = 0$ changes from a minimum to a maximum and P(s) rapidly changes (red line) (**Supplementary Fig. 1**). At the critical point, low and high synchrony networks are equally probable.

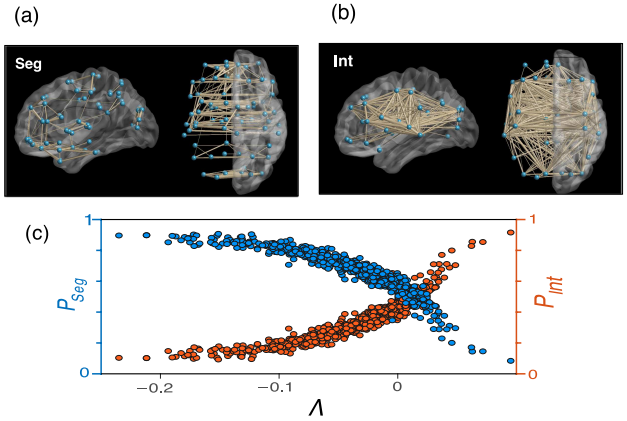

Figure 2 Λ controls the balance between segregated (low s) and integrated (high s) networks. (**a,b**) Inter-subject average functional connectivity (Pearson Correlation) during low (**a**) and high (**b**) synchrony, here visualized using the BrainNet Viewer showing the top 10 % of connections [17]. (**a**) Low synchrony ($s = 0$) reflects segregation (Seg). (**b**) High synchrony ($|s| > 1/2$) reflects integration (Int). (**c**) The fraction of time each subject (each data point and their specific value of Λ) spends in integrated (P_{Int}, orange) and segregated (P_{Seg}, blue) networks. Time spent was calculated from a bivariate regression of the functional connectivity (here over all s, from each subject) with the patterns, Seg and Int. $\Lambda < 0$ corresponds to large P_{Seg} and small P_{Int} while $\Lambda > 0$ corresponds to the opposite. The cross-over in (**c**) occurs at the critical point, $\Lambda = 0$.

works ($s = 0$) are most likely (**Fig. 1**). Much like water at its boiling point, which discontinuously changes from liquid to vapor, the switch between these cases is sharp and occurs at an intermediate coupling, called the *critical point*. Here we use Λ to denote the relative distance from a critical point. While both ordered and disordered networks are equally likely at the critical point ($\Lambda = 0$), small changes in the couplings lead to large changes in the occupation probabilities.

Our model explains the changes in observed FC patterns in terms of relative amounts of underlying segregated versus integrated activity. This is possible due to a direct correspondence between these activity patterns and synchrony. During periods of low synchrony, functional connections are found to be sparse and segregated (**Fig. 2a**, Seg), while during high synchrony, they are dense and integrated (**Fig. 2b**, Int) [5]. Consequently, just as with synchrony (**Fig. 1**), different values of Λ change the relative time spent in segregated (P_{Seg}) and integrated (P_{Int}) networks (**Fig. 2c**, $R^2 > 0.9$, sigmoidal fit not shown, each colored marker is a subject), independent of age or available energy. When $\Lambda < 0$, low synchronies and segregated networks occur more frequently, while the opposite holds when $\Lambda > 0$. In both cases, this balance rapidly shifts at the critical point, $\Lambda = 0$.

Changes in FC with both age and available energy can be described by changes in the region-region coupling Λ. Two principal findings here are that: (1) Λ significantly decreases with age ($p = 1.7 \times 10^{-38}$), and (2) Λ increases upon switching from a lower-energy glucose to higher-energy ketone metabolism ($p = 1.2 \times 10^{-3}$) (**Extended Data Fig. 3**). Here Λ, by toggling the relative frequencies of segregated and integrated networks, reflects an average cost of functional activity and, as suggested by our metabolic experiment, the amount of energy available to the brain. Thus one way the brain may conserve energy when this amount of energy available is decreased, such as through aging, is by decreasing Λ.

But why does a small change in energy availability lead to the dramatic changes in FC seen in older age? A third principal finding here is that young healthy brains are poised at a *critical point*, whereby very small changes in the coupling strength between regions leads to a sharp transition between integrated and segregated networks [13, 14]. **Figure 3** expresses this in terms of the probability distribution of s, now viewed from the top-down. Here younger brains (green) are near the critical point (black), allowing them to access both high and low synchrony networks. But as Λ decreases slightly, such as in older brains (yellow), the probabilities of higher synchrony networks quickly fall to 0.

That brains at their presumed peak of functionality should be poised so close to a critical point of synchrony may reflect a cost-benefit trade-off. If interactions were too weak (negative Λ, unimodal distributions around

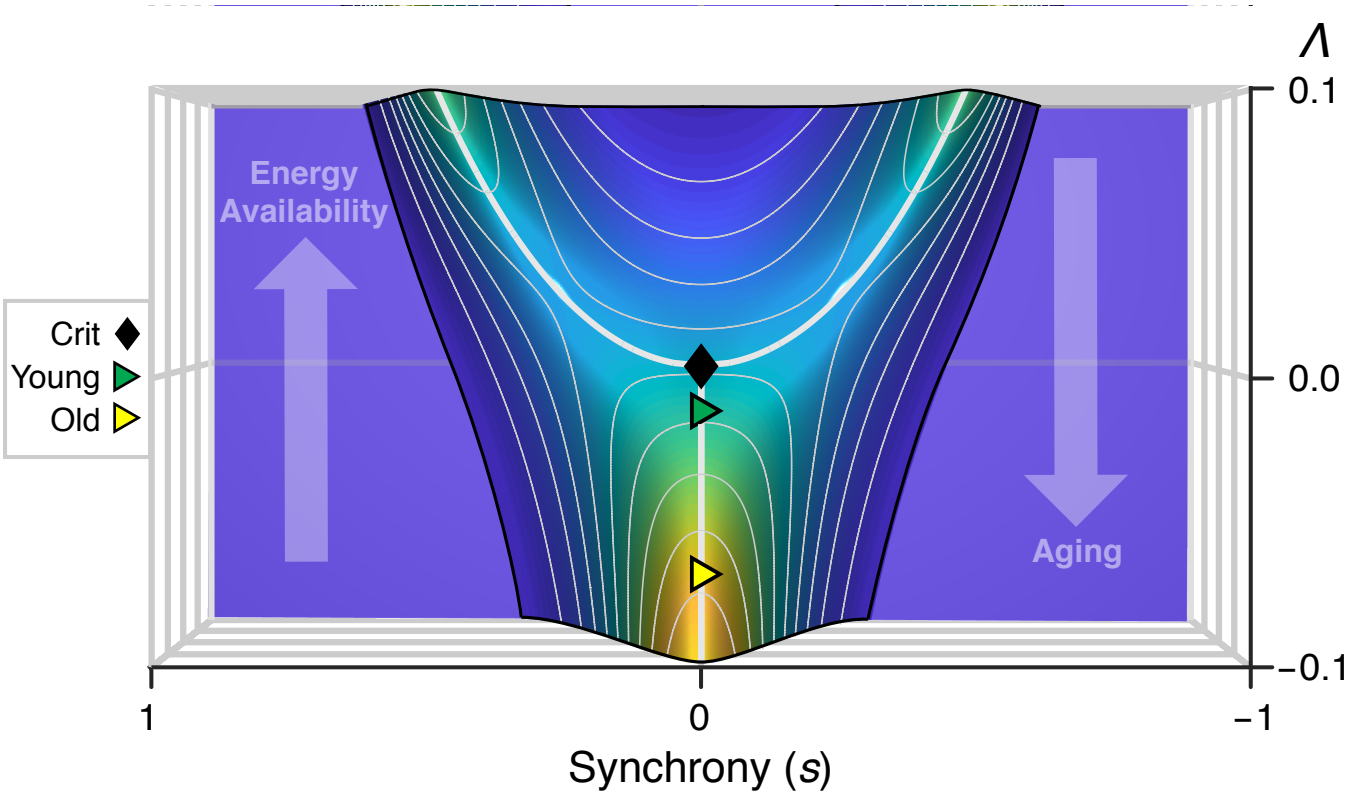

Figure 3 Younger brains are poised at a critical point; this is disrupted by decreasing energy availability. Shown is the probability distribution of synchrony (s) vs Λ, viewed from the top-down. At the critical point ($\Lambda = 0$, black), peak synchrony (indicated by a white line) changes from low ($s = 0$) towards high ($s < 0$ and $s > 0$) values. Near this transition, such as seen in younger brains (Age 25 ± 7, $N = 85$, green), both low and high synchrony networks can be accessed. Reducing metabolic activity causes Λ to decrease. Older brains (Age 81 ± 7, $N = 121$, yellow) have smaller Λ and only access low synchrony networks. The plotted triangles correspond to median Λ values (**Extended Data Fig. 3a**).

$s = 0$, no integration), the brain would have low functionality since a typical region could not access much of the rest of the brain. In contrast, if interactions were too strong (positive Λ, bimodal distributions, large positive and negative s values, no segregation), it would be metabolically expensive to run and non-specialized. By being poised at the critical point, brains can have maximum functionality at minimal metabolic energy cost [13, 18–20]. In other words, functional connectivity can switch with high efficiency between globally integrated and locally segregated activities. At the same time, however, it makes brain activity vulnerable to metabolic disruptions. Small decreases in Λ lead to a sharp loss in integrated activity, which may contribute to the cognitive deficits seen in older age.

ONLINE METHODS

Lifespan and metabolic neuroimaging datasets

To identify fMRI synchrony across the lifespan, we analyzed a large-scale open-source 3T fMRI resting-state dataset: Cambridge Centre for Ageing and Neuroscience stage II (Cam-CAN: ages 18-88, $N = 636$) [10]. To determine how energy availability (metabolism) affects fMRI synchrony, we conducted a within-subject experiment in which young healthy adults ($N = 12$, $\mu_{age} = 28\pm$ 6.73 years; 4 female) were scanned at resting-state under two conditions: (1) *glycolytic*, following their standard diet, without fasting; and (2) *ketogenic*, following a high-fat, moderate-protein, low-carbohydrate ($<$ 50 g/day) diet for one week, by which point all participants were in ketosis ($>$ 0.6 mmol/L ketone blood concentration). For details on the glycolytic and ketogenic dietary regimes, as well as validation of their blood values and neurobiological effects as comparable to calorie-matched administration of glucose and D-β-hydroxybuterate ketone bodies, see previous work[12]. This study was approved by the Institutional Review Boards of Stony Brook University and Massachusetts General Hospital/Partners Healthcare; all participants provided informed consent.

MRI acquisition

The lifespan dataset was acquired at 3T field strength; Cam-CAN had a TR=1970 ms over 8 min 40 s (fur-

ther detail may be found in dataset documentation [10]). Our metabolic dataset was acquired at ultra-high-field (7T) field strength at the Athinoula A. Martinos Center for Biomedical Imaging. Imaging included whole brain BOLD, field map, and T1-weighted structural (MEMPRAGE) images. BOLD images were acquired using a protocol quantitatively optimized, using a dynamic phantom, for detection-sensitivity to resting-state networks [21]: SMS slice acceleration factor = 5, R = 2 acceleration in the primary phase encoding direction (48 reference lines) and online GRAPPA image reconstruction, TR = 802 ms, TE = 20 ms, flip angle = 33°, voxel size = $2 \times 2 \times 1.5$ mm, slices = 85, number of measurements = 740 in each resting-state session, for a total acquisition time of 10 minutes. Field map images were acquired using the following parameters: TR = 723 ms, TE 1 = 4.60 ms, TE 2 = 5.62 ms, flip angle = 36°, voxel size = $1.7 \times 1.7 \times 1.5$ mm, slices = 89, for a total acquisition time of 3 min 14 s. The whole-brain T1-weighted structural volumes were acquired using a conventional multi-echo MPRAGE (MEMPRAGE) sequence with 1 mm isotropic voxel size and four echoes with the following protocol parameters: TE1 = 1.61 ms, TE2 = 3.47 ms, TE3 = 5.33 ms, TE4 = 7.19 ms, TR = 2530 ms, flip angle = 7°, with R = 2 acceleration in the primary phase encoding direction (32 reference lines) and online GRAPPA image reconstruction, for a total volume acquisition time of 6 min 3 s.

MRI pre-processing

Lifespan dataset pre-processing was conducted in FMRIB Software Library (FSL; https://fsl.fmrib.ox.ac.uk/fsl/fslwiki/): anatomical images were skull-stripped and co-registered to Montreal Neurological Institute (MNI) templates and mean functional images. Functional images were motion and fieldmap-corrected, brain-extracted, and co-registered to MNI templates using transformations learned through the anatomical image. Metabolic dataset pre-processing used Statistical Parametric Mapping 12 (SPM12; https://www.fil.ion.ucl.ac.uk/spm/software/spm12/). Anatomical images (MEMPRAGE) were normalized to MNI templates using unified segmentation and registration. Images of each individual participant were realigned to account for head movements, and fieldmap-corrected for geometric distortions caused by the magnetic field inhomogeneity, followed by normalization to MNI space. We did not apply spatial smoothing or global signal regression to pre-processing of either dataset. For all datasets, voxelwise data were parceled in the Willard 499 functional regions of interest (ROI) [15]. Of these, we used the 498 regions corresponding to entirely grey matter voxels.

Ising model

Here we use the principle of maximum entropy [14, 16] to build the minimally biased probability distribution of N binary (+1 or −1) node weights, $\{\hat{v}_i\}$ satisfying fixed constraints on the mean (0) and variance, $Var(s)$ of the global property, $s(\{\hat{v}_i\}) = N^{-1}\sum_{i=1}^{N}\hat{v}_i$ (synchrony). This is given by [16]:

$$P(\{\hat{v}_i\}) = Z^{-1}e^{N^2\lambda s(\{\hat{v}_i\})^2} \tag{1}$$

where Z is the partition function and normalizes the distribution. Here λ represents the average node-to-node interaction strength and is the basic mechanistic quantity of our model (**Supplementary Fig. 1a, left**). Small values of λ describe networks in which interactions between nodes are weak and in which the node weights are independent of each other. In contrast, large values of λ describe networks in which interactions between nodes are strong and node activities are highly correlated (**Supplementary Fig. 1a, right**). A given value of synchronization s may be obtained in many different ways; *ie,* it is *degenerate* (**Supplementary Fig. 1b**). In other words, since there are $\binom{N}{N(1+s)/2}$ different ways to have $s = N^{-1}\sum_i \hat{v}_i$, we find that the total probability of each synchrony $P(s)$ is:

$$P(\{\hat{v}_i\}) = Z^{-1}\binom{N}{N(1+s)/2}e^{N^2\lambda s(\{\hat{v}_i\})^2} \tag{2}$$

Therefore, when λ is small, $P(s)$ is determined by the degeneracy and low synchrony is most probable. Conversely, when λ is large, $P(s)$ is determined by the interactions between nodes and high synchrony is most probable. In particular, as the λ is varied, the relative importance of each of these terms changes. As can be seen in **Supplementary Fig. 1c**, this causes $P(s)$ to change from a bimodal (left) to a unimodal (right) distribution as depending on λ. The critical point, λ_c, is the value of λ where this shift happens (i.e. when these two contributions are balanced).

Finding the critical point

The critical point of the Ising model occurs when the degeneracy and interaction terms in **Online Methods Eq. 2** are of equal magnitude. Using the standard approximation of the binomial coefficients, $P(s)$ becomes:

$$P(s) \approx Z^{-1}\binom{N}{N/2}e^{[\lambda - \frac{1}{2N}]s^2} \tag{3}$$

Conceptually, when $\lambda < \lambda_c$, P(s) opens downwards like a Gaussian; $s = 0$ is most probable. However, when $\lambda > \lambda_c$, $P(s)$ opens upwards and large values of s (both positive and negative) are most probable. When $N = 498$

(the number of regions), we find that this critical point is $\lambda_c = \frac{1}{2N} = 1.004 \times 10^{-3}$, coinciding with the observed critical point between unimodal and bimodal synchrony (**Fig. 1**). To simplify our analysis, now refer to the rescaled coupling Λ: $\Lambda = (\lambda - \lambda_c)/\lambda_c$.

fMRI binarization

Here we access the time-dependent network properties of our data by binarizing fMRI time series. This method simplifies time series while preserving their correlation patterns. In particular, the Pearson correlation (or functional connectivity), $\rho(X, Y)$ is widely used to estimate the strength of the interaction between arbitrary pairs of variables (X,Y):

$$\rho(X, Y) = \frac{Cov(X, Y)}{\sqrt{Var(X)Var(Y)}}. \tag{4}$$

Here variables (X and Y for example) are the nodes of a graph and ρ is the weight of the edge between them. However, these interactions often change over time. Inspired by recent methods, we calculate ρ over each pair of successive time points, reducing **Online Methods Eq. 4** to [22]:

$$\rho^*(X, Y, t) = \frac{\Delta X(t)\Delta Y(t)}{\sqrt{(\Delta X(t))^2(\Delta Y(t))^2}} = \hat{X}(t)\hat{Y}(t) \tag{5}$$

$$BDM(X, t) = \hat{X}(t) \tag{6}$$

where $\hat{X}$ and $\hat{Y}$ are the signs of the time derivatives of X and Y respectively and the time-dependent correlation, ρ^*, is their product. This procedure takes our original time series $X(t)$ and produces a simplified, binarized time series $\hat{X}(t)$ (*Binarized Derivative Method*, BDM). As validation of this method, we find that this simplified representation preserves fMRI correlation patterns across time (**Supplementary Fig. 3a**) and for different subjects (**Supplementary Fig. 3b**). This approach has two key advantages over previous methods. First, it simplifies complex, many-variable interactions in terms of dynamical patterns of binary (+1 and −1) variables. Second, it is naturally compatible with Ising-like models, which have been shown to be powerful tools in isolating latent relationships within networks of neurons [14, 16].

Model fitting

Here we describe how we fit the Ising model to our data (**Supplementary Fig. 2**). First, we took the fMRI signal $v_i(t)$ for each region i and time t and binarized it using BDM. The model assumes that all nodes have, on average, similar correlation patterns. From these signals, we found that most nodes are primarily positively correlated, while a few nodes were primarily negatively correlated with other nodes. For the latter, we flipped ($\hat{v}_i \to -\hat{v}_i$) for these regions only (**Extended Data Fig. 1**). We then averaged the signals from all (498) regions of the brain to compute each subject's time-dependent *synchrony* $s(t)$. We then took the histogram of s for each subject to get a distribution $P(s)$, giving the variation in synchrony per individual. Finally, the Bayesian posterior distribution $P(\Lambda|\text{Data})$, which captures the relative quality of of our model, was used to find the best fit value and approximate error bars for Λ for each subject. Here we use a uniform (unbiased) prior distribution of Λ; thus the posterior is computed directly from the likelihood function $\mathcal{L}(\Lambda|\text{Data})$ of our Ising model **Online Methods Eq. 2.**

Statistical analysis

Binarized functional data from our lifespan and metabolic datasets were fit to the Ising model using Maximum Likelihood estimation. We determined confidence intervals for each fit using a conservative .01 likelihood ratio. We found Λ to decrease significantly with age ($p = 1.7 \times 10^{-38}$, $N = 636$) using a Spearman-rank Permutation test (since the relationship between age and Λ appeared nonlinear). Additionally we found Λ to increase significantly for the ketogenic diet, as compared to a glycolytic diet, using a Wilcoxon 1-sided signed rank test ($p = 1.2 \times 10^{-3}$, $N = 12$).

Life sciences reporting summary

Further information on experimental design is available in the Life Sciences Reporting Summary.

Data and code availability

Lifespan fMRI data are publicly available from Cam-CAN [10]. Metabolic fMRI data are located at Data Archive for the Brain Initiative (DABI: https://dabi.loni.usc.edu/explore/project/42) in the Protecting the Aging Brain (PAgB), Project 1926781 repository. Additional details (including links to custom MATLAB and Python codes used in the processing and analyses of data) can be found at http://www.lcneuro.org/software-and-instrumentation.

ACKNOWLEDGMENTS

The research was funded by the WM Keck Foundation (LRMP, KD), the NSF BRAIN Initiative (LRMP, KD: ECCS1533257, NCS-FR 1926781), and the Stony Brook University Laufer Center for Physical and Quantitative Biology (KD).

AUTHOR CONTRIBUTIONS

LRMP designed the experiments. AA pre-processed the data. CW did the modeling and designed the methods used. CW, LRMP, and KD wrote and revised the paper.

COMPETING INTERESTS

The authors declare no competing financial interests.

[1] Andrews-Hanna, J. R. et al. *Neuron.* **56**, 924–935 (2007).
[2] Geerligs, L., Renken, R. J., Saliasi, E., Maurits, N. M., and Lorist, M. M. *Cerebral cortex.* **25**, 1987–1999 (2015).
[3] Mosconi, L. *Clin. Transl. Imaging.* **1**, 217–233 (2013).
[4] Bullmore, E. and Sporns, O. *Nat. Rev. Neurosci.* **13**, 336–349 (2012).
[5] Zalesky, A., Fornito, A., Cocchi, L., Gollo, L. L., and Breakspear, M. *Proc. Natl. Acad. Sci.* **111**, 10341–10346 (2014).
[6] Friston, K. J. *Science.* **326**, 399–403 (2009).
[7] Sporns, O. *Current opinion in neurobiology.* **23**, 162–171 (2013).
[8] Tomasi, D., Wang, G. J., and Volkow, N. D. *Proc. Nat. Acad. Sci.* **110**, 13642–13647 (2013).
[9] Tomasi, D. and Volkow, N. D. *Molecular psychiatry.* **17**, 549–558 (2012).
[10] Taylor, J. R. et al. *Neuroimage.* **144**, 262–269 (2017).
[11] Sato. K. et al. *The FASEB Journal.* **9**, 651–658 (1995).
[12] Mujica-Parodi, L. R. et al. *Proc. Nat. Acad. Sci.* **117**, 6170–6177 (2020).
[13] Mora, T. and Bialek, W. *J. Stat. Phys.* **144**, 268–302 (2011).
[14] Schneidman, E., Berry, M. J., Segev, R., Bialek, W. *Nature.* **440**, 1007–1012 (2012).
[15] Altmann, A., Ng, B., Landau, S. S., Jagust, W. J., and Grecius, M. D. *Brain.* **138**, 3734–3746 (2015).
[16] Tkacik, G. et al. *PLoS Comp. Biol.* **10**, (2014).
[17] Xia, M., Wang, J., and He, Y. *PLoS One.* **8**, (2013).
[18] Beggs, J. M. *Phil. Trans. R. Soc. A.* **366**, 329–343 (2008).
[19] Cocchi, L., Gollo, L. L., Zalesky, A., and Breakspear, M. *Prog. Neurobiol.* **158**, 132–152 (2017).
[20] Chialvo, D. R. *Nat. Phys.* **6**, 744–750 (2010).
[21] DeDora, D. J. et al. *Front. Neurosci.* **10**, 180 (2016).
[22] Hutchison, R. M. et al. *Neuroimage.* **80**, 360–378 (2013).
[23] Dommers, S., Giardina, C., Giberti, C., van der Hofstad, R., and Prioriello, M. L. *Commun. Math. Phys.* **348**, 221–263 (2016).

EXTENDED DATA AND SUPPLEMENTAL FIGURES

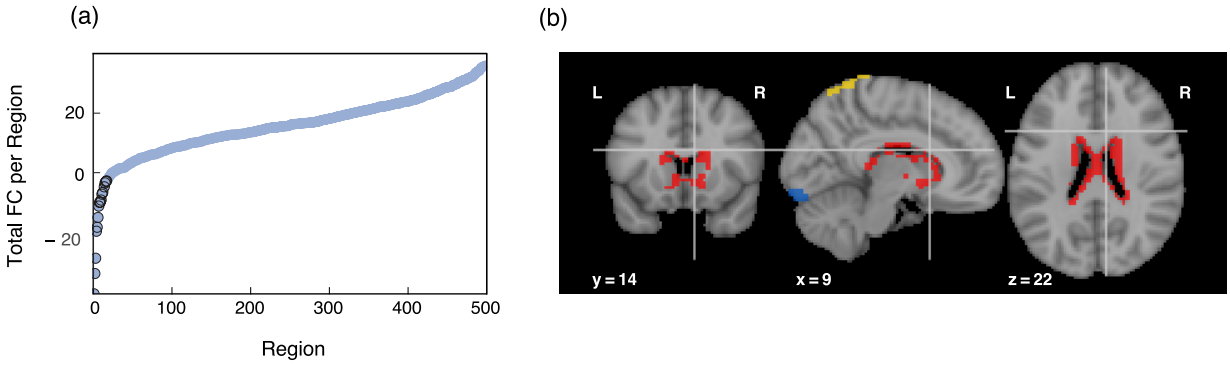

Extended Data Figure 1 Resting-state functional connectivity (FC) separates the brain into two clusters: positive and negative. (**a**) The population-averaged ($N = 636$ subjects) total functional connectivity of each region (498 in total, summed over the remaining 497 pairs) ordered from smallest to largest. The 16 leftmost regions (black highlighted circles) form the negative cluster, while the remaining majority form the positive cluster. (**b**) A three plane view of the negative (colored) regions. The negative cluster included various subcortical regions (thalamus, the fornix of the hippocampus, and the caudate nucleus in red), the supplementary motor area (yellow) and the lingual gyrus (blue). Our pre-processing excluded all non-grey matter voxels for each subject. Thus, while these regions are near grey matter borders, they were not an artifact of pre-processing.

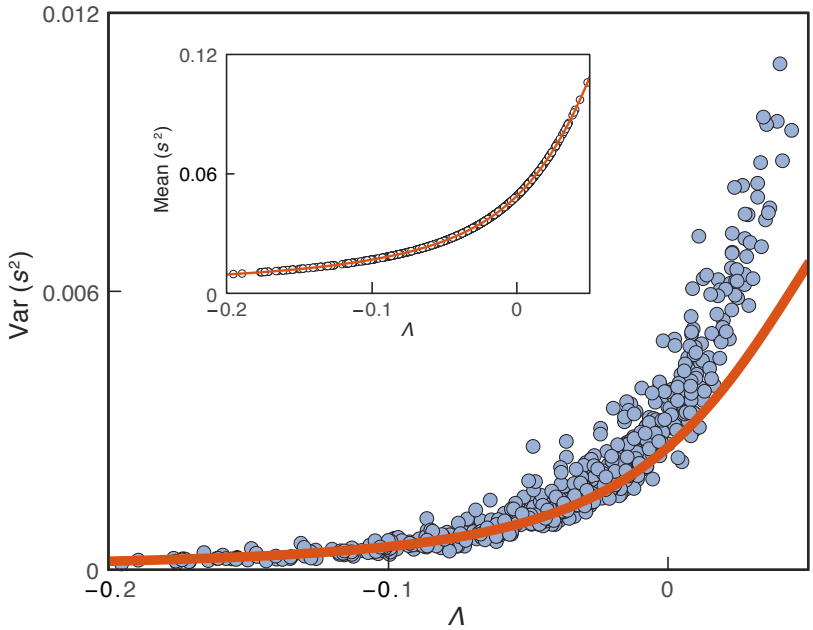

Extended Data Figure 2 The Ising model predicts higher-order features of functional data. We fit binarized functional data from our lifespan and metabolic datasets to the model using Maximum Likelihood estimation. Shown are fourth moments of synchrony $Var(s^2)$, as predicted by the model (orange), compared to experimental data (each marker is a subject). In addition to the second moment Mean(s^2), which is perfectly fit by design (inset), the model captures well the value of this additional feature sufficiently far up to $\Lambda > 0$ to be relevant to all the biological data we study here. Additionally, these deviations do not affect the important quantitative features of our model [23].

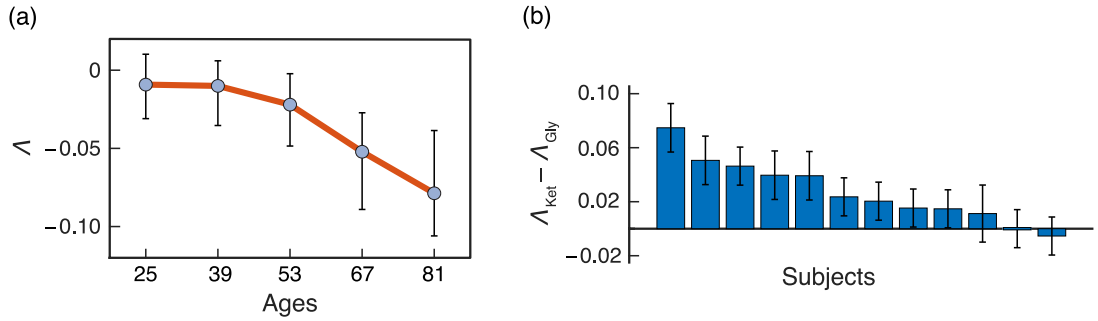

Extended Data Figure 3 Λ significantly decreases with age (**a**, $p = 1.7 \times 10^{-38}$) and increases with available energy (**b**, $p = 1.2 \times 10^{-3}$). (**a**) Here each point (as well as the orange curve connecting them) reflect the median best-fit Λ values for each (of 5) equal width (14 years) age groups. Error bars represent the upper and lower quartiles. We used a Spearman-rank Permutation test ($N = 636$, $\rho(634) = -0.48$) to test significance of the nonlinear relationship between Λ and age. (**b**) Change in Λ for each subject ($N = 12$, $W = 3$) when switching from a lower-energy glucose (glycolytic, Gly) to higher energy ketone (Ket) metabolism. Error bars reflect a .01 likelihood ratio confidence interval. A Wilcoxon 1-sided signed rank test ($N = 12$) was used to test if ketones significantly increased Λ.

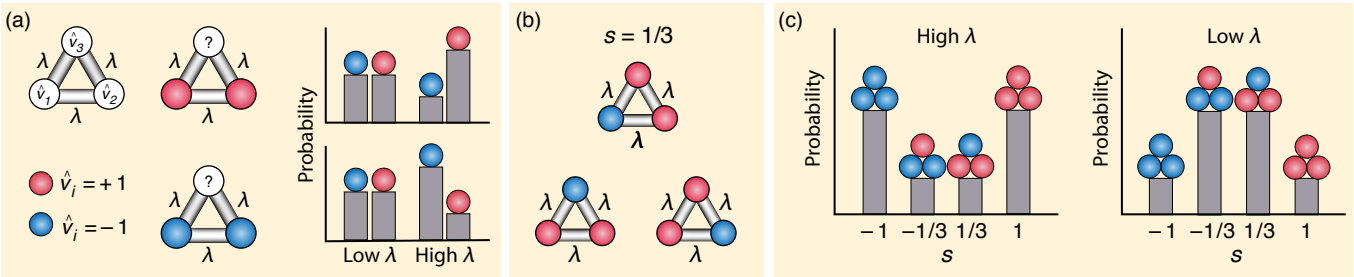

Supplementary Figure 1 The Ising model predicts network probabilities from interactions between its nodes. (**a**) The Ising model maps binary variables onto a fully-connected network (**left**). Each variable ($i = 1,2,\ldots$ N) is a node with binary weight $\hat{v}_i$ (represented by the colors red and blue), and each pair of nodes is connected by an edge with weight λ. Here we show the example of $N = 3$. The value of λ (> 0) describes the average interaction strength between nodes; the larger λ is, the more likely the unknown value of $\hat{v}_3$ is to be similar to its neighbors (**right**). (**b,c**) The probability of each network is determined by its synchrony (s). (**b**) Multiple graphs give the same value of synchrony. Since there are 3 ways to have 1 blue node and 2 red nodes, there are 3 different graphs that give $s = 1/3$ (red minus blue divided by $N = 3$). This *degeneracy* effectively triples the probability of $s = 1/3$. (**c**) The probability distribution of s given by the Ising model is a function of λ and degeneracy. When λ (interaction) is high, the probability that $|s| = 1$ is large (**left**). But, when λ is low, degeneracy wins out and the probability that $|s| = 1/3$ is large (**right**).

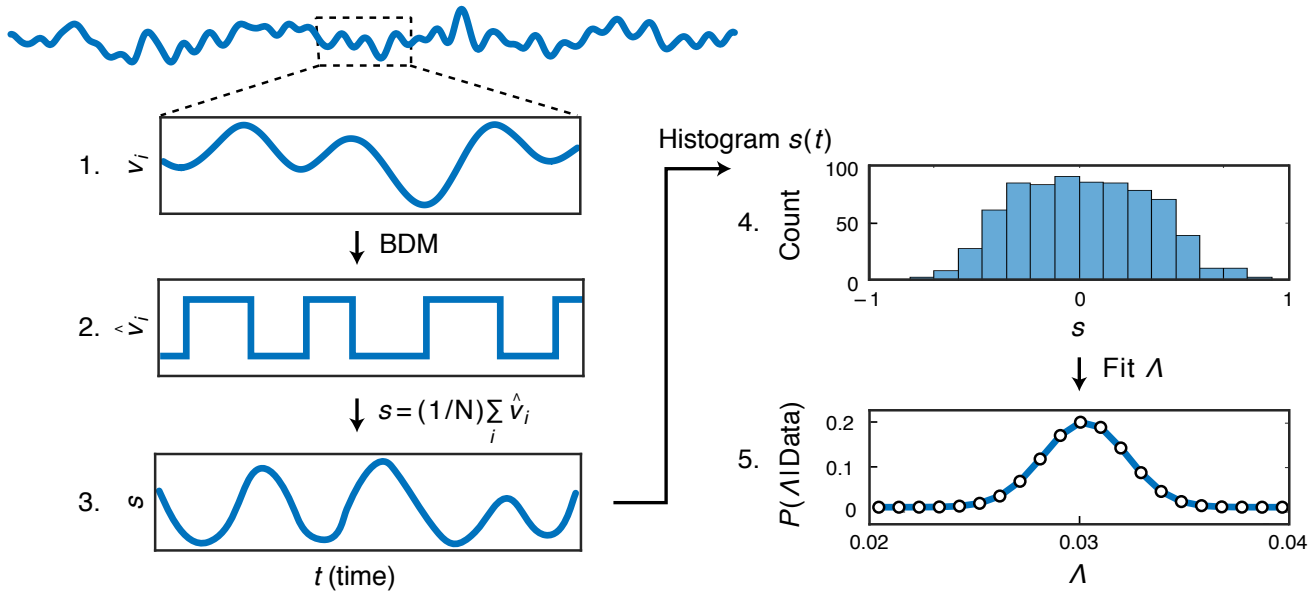

Supplementary Figure 2 How we obtain the Ising model parameter Λ from fMRI data. [1] shows the fMRI signal $v_i(t)$ from the ith brain region (out of 498), as a function of time t. [2] We binarize it, to give $\hat{v}_i(t)$. [3] The binarized signals are then averaged over all brain regions, giving that individual's time-dependent *synchrony* $s(t)$. [4] We then histogram into $P(s)$ the different s values over time [4], to express the variations in an individual's synchrony levels. [5] We then find the value of Λ that best fits $P(s)$ for each individual. Here $P(\Lambda|\text{Data})$ expresses the Bayesian posterior probability (with a uniform prior distribution over Λ) that our data $P(s)$ was generated from an Ising model (**Online Methods Eq. 2**) with relative interaction strength Λ.

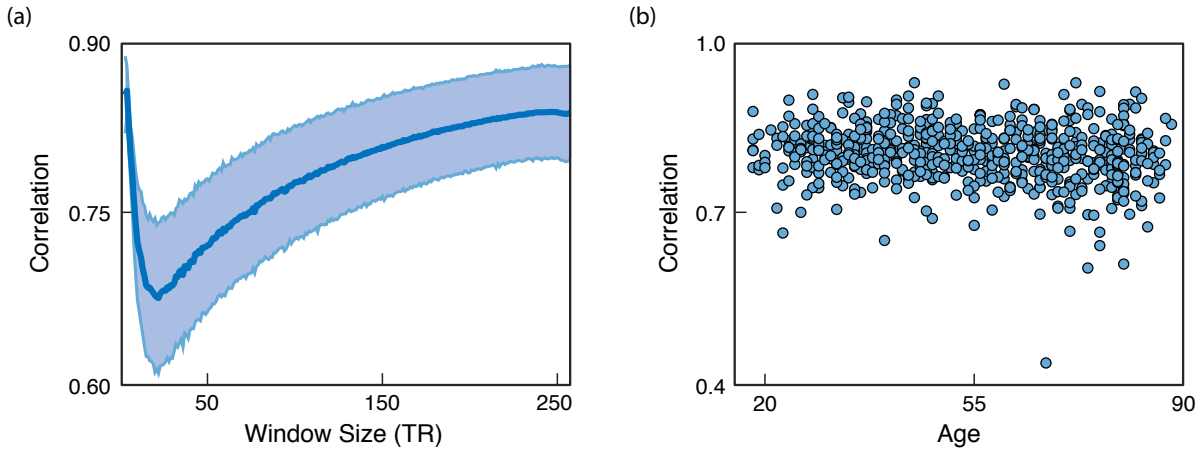

Supplementary Figure 3 Functional Connectivity (FC) can be recovered from simple, binarized signals (BDM). (**a**) The correlation between FC calculated using raw and binarized data across different windows of time. Error bars represent the population standard deviation ($N = 636$). (**b**) The same correlations (using the maximum window size) plotted against age.